PHYSICS

Magnetic excitation and readout of methyl group tunnel coherence

M. Šimėnas[1]*, D. Klose[2]*, M. Ptak[3], K. Aidas[1], M. Mączka[3], J. Banys[1], A. Pöppl[4], G. Jeschke[2†]

Methyl groups are ubiquitous in synthetic materials and biomolecules. At sufficiently low temperature, they behave as quantum rotors and populate only the rotational ground state. In a symmetric potential, the three localized substates are degenerate and become mixed by the tunnel overlap to delocalized states separated by the tunnel splitting ν_t. Although ν_t can be inferred by several techniques, coherent superposition of the tunnel-split states and direct measurement of ν_t have proven elusive. Here, we show that a nearby electron spin provides a handle on the tunnel transition, allowing for its excitation and readout. Unlike existing dynamical nuclear polarization techniques, our experiment transfers polarization from the electron spin to methyl proton spins with an efficiency that is independent of the magnetic field and does not rely on an unusually large tunnel splitting. Our results also demonstrate control of quantum states despite the lack of an associated transition dipole moment.

INTRODUCTION

Methyl groups serve as ideal systems for studying both classical and quantum regimes of molecular dynamics. The nature of methyl group motion around its symmetry axis is determined by the interplay of its rotational potential and temperature. At temperatures above the rotation barrier, methyl groups exhibit classical stochastic reorientation, which ceases at low temperature. However, because of the Heisenberg uncertainty, the wave functions of the three localized states extend into the barriers and overlap, allowing quantum rotational tunneling of methyl groups. The tunnel overlap lifts the degeneracy of the three stationary methyl group states that correspond to the minima of the rotation potential to the symmetric A ground state and antisymmetric degenerate E_A and E_B excited states (*1*). The tunnel splitting ν_t between these states is highly sensitive to the height of the barrier and can reach into the gigahertz range yet is often much smaller (*2*, *3*).

Most of methyl group tunneling studies report on the fundamental aspects of this quantum phenomenon and the ability of these groups to probe the local energy landscapes (*2*, *3*). Recently, attention has also been concentrated on the methyl quantum rotor–induced polarization (QRIP) (*4*, *5*) based on the Haupt effect (*6*), which exploits the different proton spin symmetry of the ground and excited tunneling states (*7*). However, this dynamic nuclear polarization (DNP) technique requires unusually large tunnel splittings.

In our recent work, we applied three-pulse electron spin echo envelope modulation (ESEEM) to the Mn(II)-doped hybrid perovskite framework $[(CH_3)_2NH_2][Zn(HCOO)_3]$. This experiment normally generates coherence on nuclear spin transitions by exciting subsequently an allowed electron spin transition and a formally forbidden electron-nuclear spin transition that is weakly allowed at sufficiently low fields. By observing evolution of such coherence, the nuclear magnetic resonance (NMR) spectrum of a paramagnetic compound can be obtained, and hyperfine couplings can be measured that are unresolved in electron paramagnetic resonance (EPR) spectra. In our particular case, at a measurement temperature of 10 K, we encountered signals whose frequency and modulation depth did not depend on a magnetic field between 0.325 and 3.35 T (*8*) and thus cannot be NMR lines. Neither can these signals arise from any magnetic field–dependent level mixing. Modulation depth decreased above 30 K, and the signals vanished at about 80 K. We speculated that they stem from tunnel splitting of the methyl groups (*9*). Tunneling sidebands have been observed in EPR spectra as early as 1972 (*10*), and the temperature dependence of the frequencies of our signals is akin to the one of methyl tunnel splitting observed by EPR (*11*) and electron nuclear double resonance (ENDOR) (*12*). For two-pulse ESEEM, tunnel modulations have been predicted (*13*) but never observed. Here, we show that these signals arise from the coherent superposition of the quantum rotor states of methyl groups. Our findings may lead to new frontiers in methyl group spectroscopy, DNP, and quantum information processing.

RESULTS

First, we investigate the origin of the field-independent three-pulse ESEEM signals of Mn(II)-doped $[(CH_3)_2NH_2][Zn(HCOO)_3]$ framework by systematic isotope substitution. The substitution of the amine or formate protons by deuterons does not affect the signals (Fig. 1). They also do not change upon nitrogen replacement by the isotope ^{15}N. However, the signals completely vanish upon substitution of the methyl protons by deuterons, allowing us to unambiguously assign them to the methyl groups of the dimethylammonium (DMA^+) cation that resides in the central cavity of the perovskite framework.

In two-pulse ESEEM, the methyl group tunnel splitting ν_t would be observed as frequency difference between allowed and formally forbidden electron spin transitions. In our three-pulse experiments, phase cycling (Fig. 2A) cancels contributions from electron spin coherence during the variable delay *t*. Hence, in analogy to the situation for nuclear spin states (*14*, *15*), the first two microwave pulses must generate a coherent superposition of tunnel-split states (Fig. 2D). This coherence gains phase during time *t* and is then transferred by the third microwave pulse to electron coherence, which refocuses to a

[1]Faculty of Physics, Vilnius University, Sauletekio av. 9, 10222 Vilnius, Lithuania. [2]ETH-Zürich, Department of Chemistry and Applied Biosciences, Vladimir-Prelog-Weg 2, 8093 Zürich, Switzerland. [3]Institute of Low Temperature and Structure Research, Polish Academy of Sciences, P.O. Box-1410, PL-50-950 Wrocław 2, Poland. [4]Felix Bloch Institute for Solid State Physics, Leipzig University, Linnéstr. 5, 04103 Leipzig, Germany.
*These authors contributed equally to this work.
†Corresponding author. Email: gunnar.jeschke@phys.chem.ethz.ch

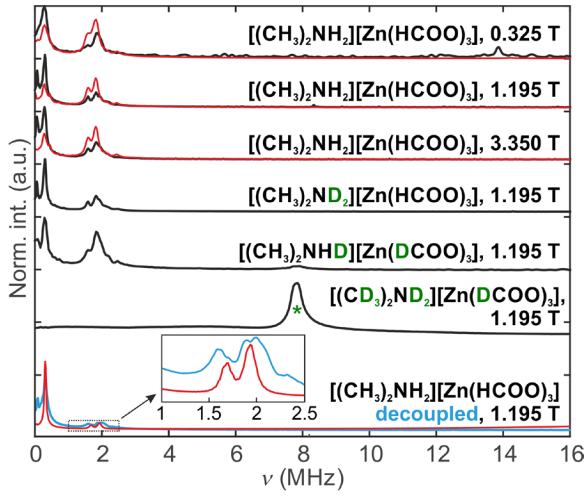

Fig. 1. Methyl tunnel signals in three-pulse ESEEM of the Mn(II)-doped hybrid perovskite framework $[(CH_3)_2NH_2][Zn(HCOO)_3]$ observed at 10 K. The signal at 7.8 MHz marked with a green asterisk stems from ^{2}H nuclear modulation. Signals below 4 MHz are field independent (top three traces) and persist upon substitution of the amine or formate protons, whereas they vanish upon substitution of the methyl protons. Signal splitting does not vanish under hyperfine decoupling (bottom trace). Experimental data are overlaid with quantum dynamics simulations (red). Norm. int., normalized intensity; a.u., arbitrary units.

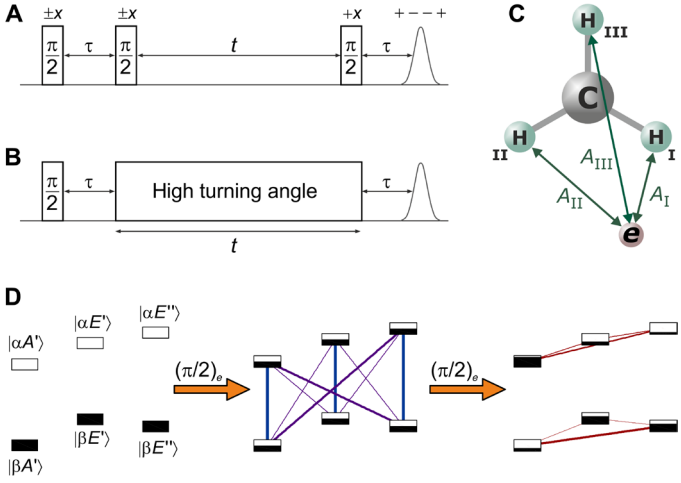

Fig. 2. Excitation and observation of tunnel coherence by microwave pulses. (**A**) Three-pulse ESEEM sequence with phase cycling indicated on top, (**B**) hyperfine-decoupled ESEEM sequence, (**C**) hyperfine-induced symmetry breaking, and (**D**) transfer of population (filling of the square boxes) and coherence (lines, thickness corresponds to amplitude) between electron spin (blue) and tunnel transitions (red) via formally forbidden transitions (violet) by the first two microwave pulses ($\nu_t = 2$ MHz and $\tau = 600$ ns).

stimulated echo. In that sense, detection of the tunnel coherence, like detection of nuclear coherence in conventional ESEEM or detection of multiple-quantum coherence in NMR experiments, is indirect. As the last transfer depends on coherence phase, echo amplitude is modulated with ν_t.

These coherence transfers require coupling of the electron spin to the quantum rotor. For a localized state, the electron spin exhibits different hyperfine couplings to the three methyl proton positions (Fig. 2C). Unless all protons are in the same spin state, this lifts degeneracy of the localized states and makes tunnel mixing electron spin dependent. When the electron spin is flipped, the local hyperfine field at the protons changes sign, causing partial excitation of tunnel transitions (see the Supplementary Materials for more details). The first microwave pulse thus excites "forbidden" electron-tunnel coherence (violet) besides allowed electron coherence (blue in Fig. 2D), and the second pulse effects transfer to tunnel coherence.

To verify the presented reasoning, we set out to simulate quantum dynamics of our experiment by density operator formalism. To that end, we consider only the $m_S = -1/2 \leftrightarrow 1/2$ EPR transition of Mn(II), which contributes most strongly to the signal and corresponds to effective electron spin $S = ½$. Adding the protons with spin $I_1 = I_2 = I_3 = ½$ and the tunnel-split states A, E_A, and E_B leads to Hilbert space dimension of 48. As tunnel and proton NMR frequencies are much smaller than the EPR frequency, the signal arises solely from thermal polarization of electron spins. Hence, the initial density operator can be written as $\sigma_0 = -\hat{S}_z$. The high-field approximation applies to the electron and the protons at 3.35 T. It can be used throughout, as the spectra are field independent. The subspace Hamiltonians $\hat{H}_\varphi$ for localized states of the methyl group with rotation phase φ are distinguished only by permutation of the hyperfine couplings A_i, where i = I, II, and III runs over proton positions (Fig. 2C). They read

$$\hat{H}_{0°} = \omega_S\hat{S}_z + \omega_I(\hat{I}_{1z} + \hat{I}_{2z} + \hat{I}_{3z}) + A_I\hat{S}_z\hat{I}_{1z} + A_{II}\hat{S}_z\hat{I}_{2z} + A_{III}\hat{S}_z\hat{I}_{3z} \quad (1A)$$

$$\hat{H}_{120°} = \omega_S\hat{S}_z + \omega_I(\hat{I}_{1z} + \hat{I}_{2z} + \hat{I}_{3z}) + A_{II}\hat{S}_z\hat{I}_{1z} + A_{III}\hat{S}_z\hat{I}_{2z} + A_I\hat{S}_z\hat{I}_{3z} \quad (1B)$$

$$\hat{H}_{240°} = \omega_S\hat{S}_z + \omega_I(\hat{I}_{1z} + \hat{I}_{2z} + \hat{I}_{3z}) + A_{III}\hat{S}_z\hat{I}_{1z} + A_I\hat{S}_z\hat{I}_{2z} + A_{II}\hat{S}_z\hat{I}_{3z} \quad (1C)$$

Tunnel overlap adds off-diagonal elements $-\nu_t/3$ that connect diagonal elements with the same spin state (m_S, m_{I1}, m_{I2}, and m_{I3}) and different rotation phase φ. Details of the simulations are discussed in the Supplementary Materials.

That the required mixing of electron spin and tunnel states, mediated by the hyperfine coupling, does occur can be seen by diagonalizing the Hamiltonian (Fig. 3A). We have included only dipole-dipole hyperfine coupling, since the DMA^+ cation is not coordinated to Mn(II). The assumed hyperfine couplings of $A_I = 2.59$, $A_{II} = 1.71$, and $A_{III} = 1.48$ MHz are expected in an arbitrary orientation and a tunnel frequency $\nu_t = 1.75$ MHz in the range where we observe the field-independent signals. The degenerate E_A and E_B levels split into E' and E'' levels, and the splitting is different for the electron α and β states. Thickness of the horizontal lines visualizes contribution of the unperturbed tunnel states A, E_A, and E_B to the hyperfine-perturbed states A', E', and E''. These contributions also differ between the electron spin α and β states, which implies that a change of the electron spin state partially excites tunnel transitions. Figure 3B shows that, for hyperfine couplings in this range, perturbation of the hyperfine multiplet and substantial amplitude of forbidden electron spin–tunnel transitions occur over two orders of magnitude of the tunnel frequency, from about 100 kHz to 10 MHz. Higher tunnel frequencies would be accessible for methyl groups that are closer to the electron spin or for larger, substantially different isotropic

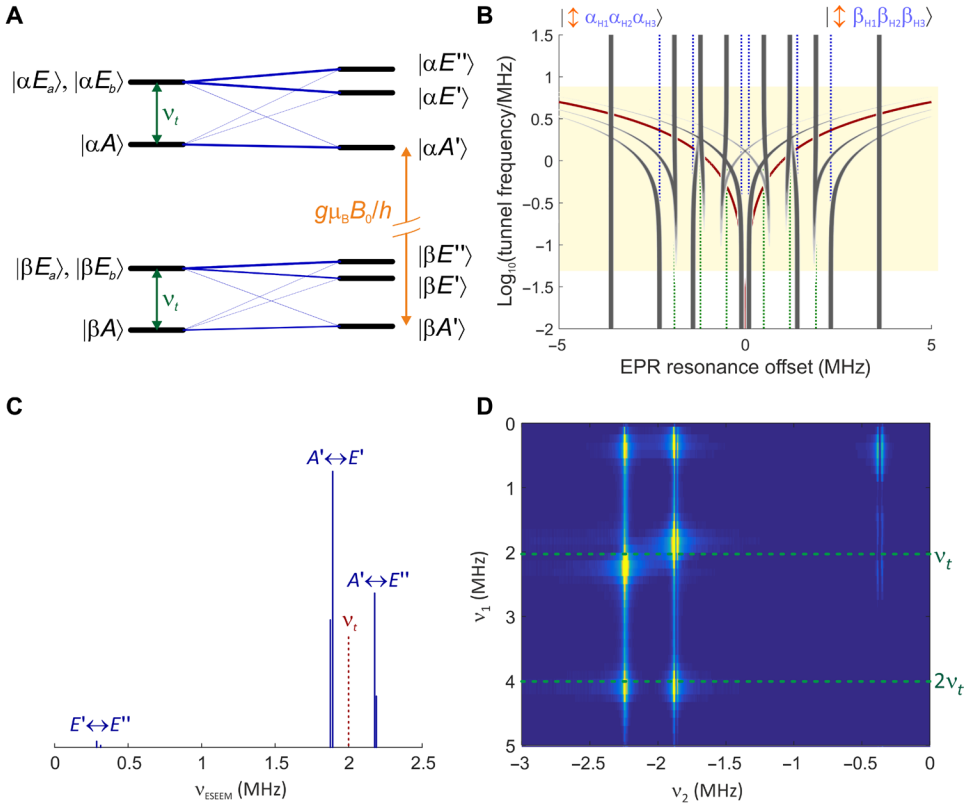

Fig. 3. Level mixing and coherence buildup in quantum rotor ESEEM. (**A**) The tunnel-split symmetry-adapted levels of the methyl group in the absence of hyperfine coupling (left) are shifted and mixed by the hyperfine perturbation (right). Thickness of the blue lines visualizes the contribution of hyperfine-unperturbed levels to the hyperfine-perturbed levels. See text for simulation parameters. (**B**) Changes in the EPR stick spectrum of three methyl protons coupled to an electron spin at a distance of approximately 4 Å when going from the tunnel-unperturbed (bottom) to the strong tunneling (top) regime (arbitrary orientation). Gray lines correspond to EPR lines with their thickness visualizing intensity. The red lines denote the tunnel frequency ($\pm\nu_t$). Dotted blue lines extrapolate the frequencies in the absence of tunnel perturbation to the strong tunneling regime, and green dotted lines extrapolate the frequencies in the large tunneling limit to the weak tunneling regime. In the pale yellow region, mixed electron-spin/tunnel transitions are weakly allowed. (**C**) Stick tunnel ESEEM spectrum corresponding to the situation shown in (A). (**D**) Simulated two-dimensional spectrum for variation of interpulse delays τ (vertical) and t (horizontal). The peaks at the hyperfine-perturbed tunnel frequencies around 2 MHz (horizontal) have buildup components at the tunnel frequency, at twice the tunnel frequency, and at the E' and E'' splitting.

hyperfine couplings to the three proton positions. As the isotropic proton hyperfine coupling cannot exceed 1.4 GHz and a nonbonded hydrogen atom cannot be closer than about 2.5 Å to an electron spin–carrying atom, corresponding to a dipole-dipole coupling of about 5 MHz, tunnel frequencies much greater than 1 GHz are probably inaccessible by this technique. On the other hand, the 190-MHz tunnel frequency in radicals generated by γ-irradiation of methyl malonic acid should be accessible provided sufficient excitation bandwidth, as, in this case, the formally forbidden electron-spin/tunnel transitions are observable even by continuous-wave EPR (*11*).

An ESEEM stick spectrum for a single orientation is shown in Fig. 3C. Coherence on the $E' \leftrightarrow E''$ transition is only weakly excited—an effect that we observe at all orientations. The $A' \leftrightarrow E'$ and $A' \leftrightarrow E''$ transitions appear close to ν_t but are split to second order by the hyperfine perturbation. The transition frequencies slightly differ between the electron spin α and β states, so that, together, six lines are expected. Because of line broadening and the low amplitude of the $E' \leftrightarrow E''$ transition, only two lines per orientation may be observable. The hyperfine-perturbative splitting between the $A' \leftrightarrow E'$ and $A' \leftrightarrow E''$ transitions depends on orientation (see Fig. 4A). Hence, a broadened and possibly structured doublet that is centered near ν_t is expected for each methyl group close to the paramagnetic center.

Only the two methyl groups closest to the Mn(II) ion are expected to contribute substantially to modulation, as the dipolar hyperfine coupling decreases with the third power of spin-spin distance. Their hyperfine couplings can be estimated from the 100-K crystal structure (*16*) using the point-dipole approximation. Thus, the two tunnel frequencies $\nu_{t,1}$ and $\nu_{t,2}$ along with the linewidth are the only free parameters. We obtain best fits with $\nu_{t,1}$ = 1.93 MHz and $\nu_{t,2}$ = 1.68 MHz for the signal around 1.75 MHz and with $\nu_{t,1} = \nu_{t,2}$ = 0.31 MHz for the low-frequency signal (Figs. 5A and 1, red lines). By the hindered quantum rotor model (*17*), the frequencies can be converted to rotation barriers E_{rot} of 10.5, 10.7, and 13.1 kJ/mol in reasonable agreement with E_{rot} = 12.3 kJ/mol predicted from the crystal structure by density functional theory (DFT). The deviation may stem from different temperatures (10 K versus 100 K) and from our system being the Mn(II)-doped Zn(II) compound, whereas the crystal structure is of the pure Mn(II) compound. The number of peaks does not change when reducing Mn(II) concentration from 0.05 to 0.005 mole percent (mol %), excluding different ion patterns in neighboring unit cells as the cause for the large number of peaks.

The necessity of using two sets of tunnel frequencies may indicate the perturbation of the tunnel frequency ν_t by electron spin

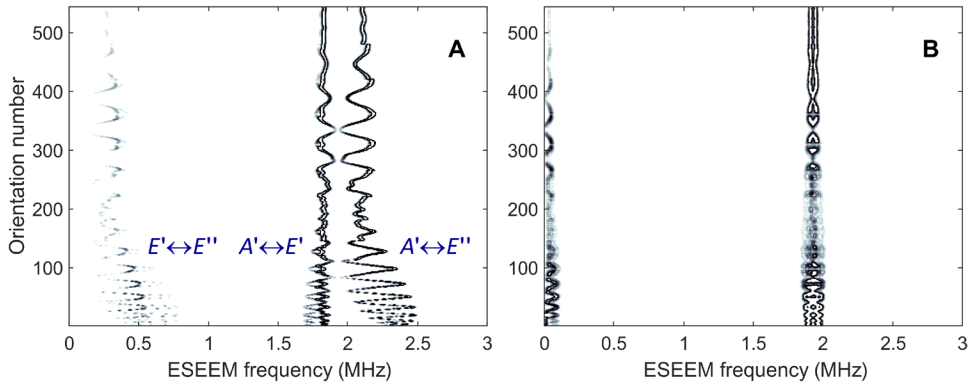

Fig. 4. Effect of hyperfine decoupling on hyperfine-perturbed tunnel spectra (simulation). (**A**) Orientation dependence of stick spectra of the type shown in Fig. 3C. Orientations on a spherical grid are spread along the vertical axis. Line amplitude is indicated by shades of gray. No decoupling. (**B**) Same orientation dependence with a decoupling field $\nu_1 = 40$ MHz. Simulations were performed for a magnetic field of 1.195 T.

admixture. Thus, we expected narrower features and reduction of the number of peaks in a hyperfine-decoupled ESEEM (Fig. 2B) (*18*) spectrum, as was also suggested by simulations (Fig. 4). However, this expectation was not borne out (bottom trace in Fig. 1).

Our simulations also predict buildup of tunnel modulation with $\sin(2\pi\nu_t\tau)$ and, to a lesser extent, $\sin(4\pi\nu_t\tau)$ and with the $E' \leftrightarrow E''$ transition frequency, when increasing interpulse delay τ, as shown by a two-dimensional spectrum (Fig. 3D) simulated by variation of τ (vertical frequency axis) and t (horizontal frequency axis). We have performed corresponding simulations with the parameters extracted above. Simulated buildup of the signal amplitude with increasing interpulse delay τ agrees nicely with experiment (Fig. 5, B and C).

In addition, the temperature dependence of the ESEEM signal (Fig. 5, D and E) can be fitted well with the Prager model (Fig. 5F) (*3*, *19*)

$$\nu_t = \nu_{t0}[1 - S_2 \exp(-E_{S2}/kT)] \quad (2)$$

According to this model the temperature dependence is dominated by a so-called shaking term (*18*) with an activation energy E_{S2}, an amplitude S_2, and the limiting tunneling frequency ν_{t0}. The process is due to interactions with phonons, which modulate the orientation of the rotational potential in the crystal lattice. Fitting each of the tunneling frequencies by the model (Eq. 2) yields the parameters given in table S1. We find that the tunneling frequencies observed at 5 and 10 K are free from temperature-induced shifts and the phonon activation energies are in the range of 1.36 to 1.41 kJ/mol.

We attempted to resolve the remaining discrepancies by studying a structurally similar Mn(II)-doped $[(CH_3)_2NH_2[Cd(N_3)_3]$ perovskite framework previously characterized by continuous-wave EPR (*20*). The crystal structure for the Cd(II) host compound is known at 150 K (*21*). Again, the three-pulse ESEEM spectrum reveals a low-frequency signal consisting of more peaks than expected (Fig. 6A), and, again, this is not rectified by hyperfine decoupling (Fig. 6, E and F). The main features can be simulated with tunnel frequencies $\nu_{t,1} = 0.73$ MHz and $\nu_{t,2} = 0.68$ MHz, corresponding to rotation barriers of 11.9 and 12.0 kJ/mol (DFT calculation based on crystal structure: $E_{rot} = 9.3$ and 11.2 kJ/mol). Similar observations on modulation buildup and temperature dependence were also made on this compound (Fig. 6, B to D).

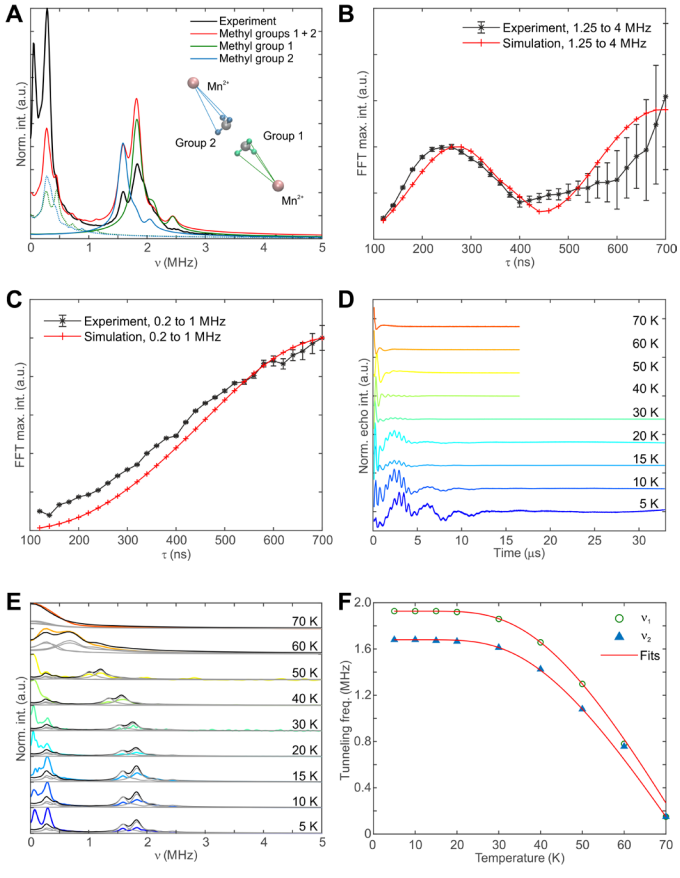

Fig. 5. ESEEM data for Mn-doped $[(CH_3)_2NH_2][Zn(HCOO)_3]$ obtained at 3.350 T. (**A**) ESEEM spectrum (black; 10 K) and its simulation (red) by the two inequivalent Mn-methyl pairs (inset) seen in the 100-K crystal structure. Component spectra shown in blue and green assume that each pair contributes with two tunnel frequencies. (**B**) Experimental (black; 10 K) and simulated (red) dependence of signal amplitude on first interpulse delay τ (tunnel frequency around 1.75 MHz). FFT, fast Fourier transform. (**C**) Experimental (black; 10 K) and simulated (red) dependence of signal amplitude on first interpulse delay τ (tunnel frequency of 0.31 MHz). (**D**) Time-domain data for temperature dependence. (**E**) Spectra for temperature dependence (colored) and simulation by two components (black and gray). (**F**) Temperature dependence of the tunnel frequency and fit by the Prager model.

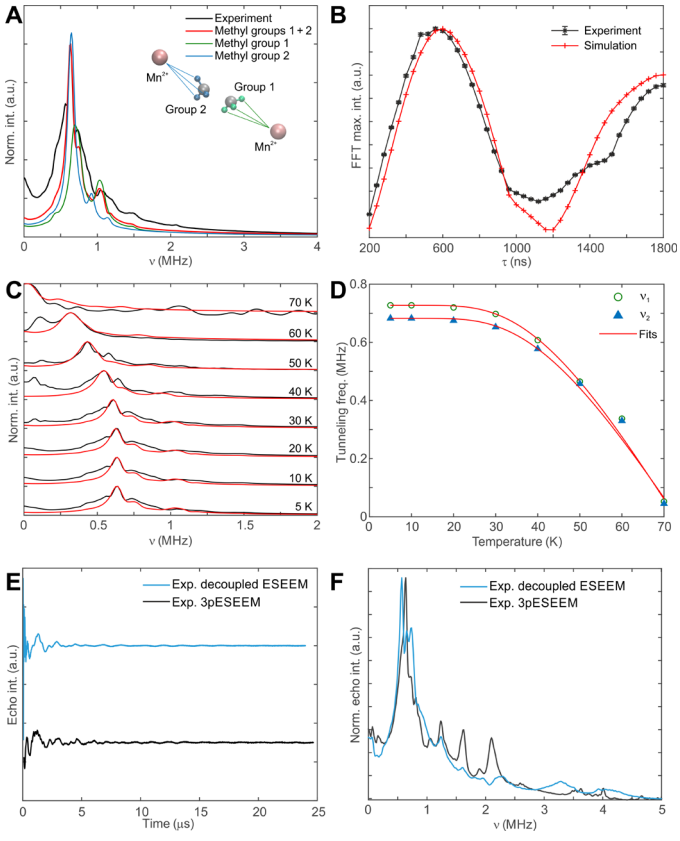

Fig. 6. Methyl tunneling in Mn(II)-doped $[(CH_3)_2NH_2][Cd(N_3)_3]$. (**A**) Experimental (black; 10 K) and simulated (colored) W band (3.350 T) three-pulse ESEEM spectra using tunnel frequencies of 0.73 and 0.68 MHz for the two methyl groups (green and blue; see inset for arrangement). (**B**) Experimental (black; 10 K) and simulated (red) dependence of maximum intensity in the W band magnitude spectra on delay τ. (**C**) Experimental temperature dependence of the W band spectra (black) and simulations (red). (**D**) Temperature dependence of W band–detected tunnel frequencies [color code as in (A)] and fits (red) according to the Prager model. (**E**) Time-domain data acquired at 10 K with Q band (1.195 T) three-pulse ESEEM (black) and hyperfine-decoupled ESEEM (blue). (**F**) Experimental Q band three-pulse ESEEM spectrum (black) and hyperfine-decoupled ESEEM spectrum (blue) obtained at 10 K.

DISCUSSION AND CONCLUSIONS

All our observations point to tunnel splitting as the cause for the field-independent ESEEM signals, yet more peaks are observed with hyperfine decoupling than there exist inequivalent Mn(II)-CH_3 pairs (Fig. 5A). We tentatively explain this by rotational coupling between the geminal methyl groups in DMA^+. For lithium acetate dihydrate (*22*) and 4-methyl pyridine (*23*) with shallow rotation potentials, multiple tunnel transitions were observed by inelastic neutron scattering and ascribed to intermolecular rotational coupling. Recent analysis for a pair of methyl groups demonstrated that strong rotational coupling can split states even for deep rotation potentials (*24*). In such a scenario, the 0.31-MHz signal for Mn(II)-doped $[(CH_3)_2NH_2][Zn(HCOO)_3]$ could be assigned to the $E_AE_B \leftrightarrow E_AE_A$ transition. Preliminary DFT computations for an isolated DMA^+ ion in vacuum indicate notable rotational coupling of the two methyl groups. Further work is required to confirm or reject this speculation and, in particular, to understand the splitting patterns. If our interpretation is confirmed, then the tunnel spectra could not only reveal the chemical binding situation of methyl groups near an electron spin, which strongly affects the rotation barrier and thus ν_t (*3*), but also whether two or three methyl groups are bound to the same atom.

Application of such tunnel spectroscopy to structure determination may hit obstacles due to the very strong sensitivity of the tunnel frequency on the rotation barrier and, thus, on packing effects. On the other hand, the same phenomenon may provide a sensitive tool for detecting binding of, for instance, ligands to proteins, which will affect local packing. In this respect, it is of interest that active centers in metalloenzymes are often paramagnetic or can be probed by paramagnetic substitution of a diamagnetic metal ion (*25*).

Another obstacle to application is the necessity for a matching of the differences in hyperfine couplings at the three proton positions to the tunnel frequency. This leads to a rather small radius around the paramagnetic center where methyl groups are potentially detectable by this technique. Note, however, that an extensive experimental NMR and computational molecular dynamics study found rotation barriers between 4 and 17 kJ/mol for methyl groups in proteins (*26*), suggesting that many methyl groups should be detectable at similar distances (3.5 to 5 Å) from a paramagnetic center as in our hybrid perovskite frameworks. Methyl groups of amino acid residues or substrate molecules are not uncommon at such distances from a metal center in metalloenzymes. Furthermore, effects of methyl tunneling have been observed before in flavoproteins (*27*) and may be expected in other radical enzymes. In favorable cases, the tunnel frequency can be detected by ENDOR spectroscopy as an additional splitting of hyperfine split–nuclear spin transitions, as was demonstrated for a 1.4-MHz tunnel frequency on γ-irradiated single crystals of α-aminoisobutyric acid (*28*). However, this approach would fail for lack of resolution in our case of a microcrystalline sample and for samples available only as glassy frozen solutions.

Furthermore, our simulations indicate field-independent transfer of electron spin polarization to tunnel polarization (Fig. 2D, right), albeit with maximum orientation-averaged efficiency of only 0.3% for the ν_t = 1.93 MHz species in Mn(II)-doped $[(CH_3)_2NH_2][Zn(HCOO)_3]$ at τ = 148 ns. Optimization of the system and of subsequent polarization transfer to methyl protons, as in QRIP (*4*, *5*), may lead to a new high-field approach to DNP. If methyl groups could be addressed individually, then they might also serve as qubits (*29*) or quantum memory (*30*) for quantum information processing. On a more fundamental level, observation of tunnel-state coherence and polarization provides an opportunity to study lifetimes, decoherence, rotational coupling (*24*), and environment dependence of methyl tunnel states.

MATERIALS AND METHODS

Sample preparation

$[(CH_3)_2NHD][Zn(DCOO)_3]$: 0.05 Mn(II) (mol %) was obtained by placing 16 ml of CH_3OD solution containing 12.5 mmol of $(CH_3)_2NH$ and 12.5 mmol of perdeuterated formic acid, DCOOD, at the bottom of a glass tube. On this solution, 16 ml of CH_3OD solution containing 1.5992 mmol of $ZnCl_2$ and 0.0008 mmol of $MnCl_2$ was gently added, and the colorless crystals were harvested after 5 days. $[(CH_3)_2NH_2][Zn(HCOO)_3]$: 0.005 Mn(II) (mol %) was obtained analogously with natural isotope abundance reagents, 10 times lower amount of $MnCl_2$, and correspondingly increased amount of $ZnCl_2$.

In $[(CD_3)_2ND_2][Zn(DCOO)_3]$, 0.05 Mn(II) mol % was prepared using the same method, but the bottom solution contained 416 ml

of gaseous $(CD_3)_2ND$ and 1 g of DCOOD dissolved in 15 ml of CH_3OD. $[(CH_3)_2ND_2][Zn(HCOO)_3]$: 0.05 Mn(II) (mol %) was prepared by heating a mixture of $ZnCl_2$ (4.9975 mmol), $MnCl_2$ (0.0025 mmol), dimethylformamide (30 ml), and D_2O (30 ml) at 140°C for 48 hours in a Teflon-lined microwave autoclave. Colorless crystals were harvested from the mother liquid after 1 week. The synthesis of $[(CH_3)_2NH_2][Zn(HCOO)_3]$: 0.05 Mn(II) and $[(CH_3)_2NH_2][Cd(N_3)_3]$: 0.05 Mn(II) samples is described in (*8*, *9*), respectively.

EPR measurements

Crystals were ground by a mortar, and the powder was filled into quartz capillaries of 3-, 1.6-, or 0.9-mm outer diameter for EPR measurements at X, Q, or W band frequencies, respectively, corresponding to ca. 9.5, 34.5, and 94 GHz and fields of 0.325, 1.195, and 3.350 T, respectively. EPR experiments in X and W bands were carried out using ELEXSYS E580 and E680 spectrometers (Bruker BioSpin, Rheinstetten, Germany), respectively, equipped either with an EN4118X-MD4 resonator with a 1-kW traveling-wave tube (TWT) amplifier or with a pulse ENDOR W band resonator and a 2-W solid-state microwave amplifier. For EPR experiments in Q band, we used an ELEXSYS E680 spectrometer equipped with an EN5107D2 resonator and a 150-W TWT amplifier. Helium flow cryostats (Oxford Instruments, Oxfordshire, UK) were used to cool the sample at a rate of 1 to 2 K/min and to stabilize the temperature to 10 K unless stated otherwise. Echo-detected EPR spectra were recorded using the Hahn echo sequence $\pi/2 - \tau - \pi - \tau -$ echo, in X band with an interpulse delay τ of 200 ns and microwave pulse lengths of 16 and 32 ns for $\pi/2$ and π, respectively. Three-pulse ESEEM data were recorded in time domain by integrating the stimulated echo using the sequence $\pi/2 - \tau - \pi/2 - t - \pi/2 - \tau -$ echo using a time step of $\Delta t = 8$ ns. The external magnetic field was set to the low-field line of the central Mn(II) hyperfine sextet, and a pulse sequence repetition time of 2 ms was used. A four-step phase cycle was used to cancel unwanted echoes. At Q and W band frequencies, pulse lengths were set to 12 and 24 ns for $\pi/2$ and π pulses, respectively. For decoupled ESEEM using the pulse sequence $\pi/2 - \tau -$ high turning angle (HTA) $- \tau -$ echo with $\tau = 128$ ns, we incremented the length of the HTA pulse starting from 12 ns in steps of 4 ns with a constant pulse amplitude of 20 MHz corresponding to 12 ns = $\pi/2$. The actual $\pi/2$ pulse had a length of 48 ns and thus narrower bandwidth to avoid poor decoupling at large resonance offsets. A $[+x] - [-x]$ phase cycle was used to cancel receiver offsets. Three-pulse ESEEM data for comparison with hyperfine-decoupled ESEEM were obtained with $\tau = 128$ ns. For data analysis, ESEEM time domain data were baseline corrected by dividing by a stretched exponential function, subsequently apodized by a Hamming window function {or by a Dolph-Chebyshev window in case of Mn(II)-doped $[(CH_3)_2NH_2][Zn(HCOO)_3]$}, zero-filled to four times the number of initial data points and Fourier transformed with cross-term averaging (*31*) to prevent spectral distortions due to experimental dead times at the beginning the time traces. All steps were carried out using home-written MATLAB (The MathWorks Inc., Natick, MA) scripts.

Quantum dynamics computations

Computations by density operator formalism were implemented in home-written MATLAB (The MathWorks Inc., Natick, MA) scripts. Spin-operator matrices were generated by the sop function and orientation grids for averaging with the sphgrid function of EasySpin version 5.2.13 (*32*). Propagators for fixed delays and for one increment of the variable delays were computed with the expm function of MATLAB. A detailed description is provided in the Supplementary Materials.

DFT computations and prediction of tunnel splittings

The DFT calculations of the rotation barriers of methyl groups in $[(CH_3)_2NH_2][Zn(HCOO)_3]$ and $[(CH_3)_2NH_2][Cd(N_3)_3]$ were performed using the experimental crystal structures reported in (*16*, *20*). First, the geometry of the DMA^+ cation was optimized by keeping the rest of the framework fixed. Then, the potential energy scans were performed by separately rotating each methyl group and allowing other degrees of freedom of DMA^+ and its position to relax. The calculations were performed using a B3LYP functional along with a cc-pVTZ basis set for DMA^+ cation and anionic linkers and a LanL2DZ pseudopotential for metal ions. All calculations were carried out using Gaussian 09 (*33*).

For the prediction of tunnel splittings, the Hamiltonian was set up in a basis of eigenstates of the free quantum rotor and diagonalized (*17*). The tunnel splitting was taken as the energy difference between the two lowest-energy states. We found that the procedure was safely converged with respect to basis size when using 301 basis states. An assessment of potential rotational couplings between the geminal methyl groups in the DMA^+ cation was made using ORCA (*34*).

SUPPLEMENTARY MATERIALS

Supplementary material for this article is available at http://advances.sciencemag.org/cgi/content/full/6/18/eaba1517/DC1

REFERENCES AND NOTES

1. A. Horsewill, Quantum tunnelling aspects of methyl group rotation studied by NMR. *Prog. Nucl. Magn. Reson. Spectrosc.* **35**, 359–389 (1999).
2. L. H. Spangler, Structural information from methyl internal rotation spectroscopy. *Annu. Rev. Phys. Chem.* **48**, 481–510 (1997).
3. M. Prager, A. Heidemann, Rotational tunneling and neutron spectroscopy: A compilation. *Chem. Rev.* **97**, 2933–2966 (1997).
4. M. Icker, S. Berger, Unexpected multiplet patterns induced by the Haupt-effect. *J. Magn. Reson.* **219**, 1–3 (2012).
5. B. Meier, J.-N. Dumez, G. Stevanato, J. T. Hill-Cousins, S. S. Roy, P. Håkansson, S. Mamone, R. C. D. Brown, G. Pileio, M. H. Levitt, Long-lived nuclear spin states in methyl groups and quantum-rotor-induced polarization. *J. Am. Chem. Soc.* **135**, 18746–18749 (2013).
6. J. Haupt, A new effect of dynamic polarization in a solid obtained by rapid change of temperature. *Phys. Lett. A* **38**, 389–390 (1972).
7. B. Zhang, C. Sun, A. M. Alsanoosi, A. Aibout, A. J. Horsewill, Spin-symmetry conversion in methyl rotors induced by tunnel resonance at low temperature. *J. Chem. Phys.* **140**, 084302 (2014).
8. M. Šimėnas, L. Macalik, K. Aidas, V. Kalendra, D. Klose, G. Jeschke, M. Mączka, G. Völkel, J. Banys, A. Pöppl, Pulse EPR and ENDOR study of manganese doped $[(CH_3)_2NH_2][Zn(HCOO)_3]$ hybrid perovskite framework. *J. Phys. Chem. C* **121**, 27225–27232 (2017).
9. L. Latanowicz, W. Medycki, R. Jakubas, The effect of low-temperature dynamics of the dimethylammonium group in $[(CH_3)_2NH_2]_3Sb_2Cl_9$ on proton spin-lattice relaxation and narrowing of the proton NMR line. *J. Phys. Chem. A* **109**, 3097–3104 (2005).
10. S. Clough, J. Hill, F. Poldy, Tunneling sidebands of methyl group hyperfine-structure. *J. Phys. C Solid State Phys.* **5**, 1739–1744 (1972).
11. S. Clough, J. R. Hill, Temperature-dependence of methyl-group tunneling rotation frequency. *J. Phys. C Solid State Phys.* **7**, L20–L21 (1974).
12. F. Bonon, M. Brustolon, A. L. Maniero, U. Segre, An ENDOR study of the temperature-dependence of methyl tunneling. *Chem. Phys.* **161**, 257–263 (1992).
13. A. R. Sørnes, N. P. Benetis, Theory of electron spin-echo envelope modulation in isotropic tunneling methyl rotor systems. *Chem. Phys. Lett.* **287**, 590–596 (1998).
14. A. Schweiger, G. Jeschke, *Principles of Pulse Electron Paramagnetic Resonance* (Oxford Univ. Press, 2001).

15. G. Jeschke, A. Schweiger, Matched two-pulse electron spin echo envelope modulation spectroscopy. *J. Chem. Phys.* **105**, 2199–2211 (1996).
16. M. Sánchez-Andújar, S. Presedo, S. Yáñez-Vilar, S. Castro-García, J. Shamir, M. A. Señarís-Rodríguez, Characterization of the order-disorder dielectric transition in the hybrid organic-inorganic perovskite-like formate $Mn(HCOO)_3[(CH_3)_2NH_2]$. *Inorg. Chem.* **49**, 1510–1516 (2010).
17. R. M. Dimeo, Visualization and measurement of quantum rotational dynamics. *Am. J. Phys.* **71**, 885–893 (2003).
18. G. Jeschke, A. Schweiger, Hyperfine decoupling in electron spin resonance. *J. Chem. Phys.* **106**, 9979–9991 (1997).
19. A. Heidemann, M. Prager, M. Monkenbusch, Methyl rotation in acetamide: The transition from quantum mechanical tunneling to classical reorientation studied by inelastic neutron scattering. *Z. Phys. B Condens. Matter* **76**, 77–88 (1989).
20. M. Trzebiatowska, M. Maczka, M. Ptak, L. Giriūnas, S. Balčiūnas, M. Šimėnas, D. Klose, J. Banys, Spectroscopic study of structural phase transition and dynamic effects in a $[(CH_3)_2NH_2][Cd(N_3)_3]$ hybrid perovskite framework. *J. Phys. Chem. C* **123**, 11840–11849 (2019).
21. Z.-Y. Du, T.-T. Xu, B. Huang, Y.-J. Su, W. Xue, C.-T. He, W.-X. Zhang, X.-M. Chen, Switchable guest molecular dynamics in a perovskite-like coordination polymer toward sensitive thermoresponsive dielectric materials. *Angew. Chem. Int. Ed.* **54**, 914–918 (2015).
22. S. Clough, A. Heidemann, A. H. Horsewill, M. N. J. Paley, Coupled tunnelling motion of a pair of methyl groups in lithium acetate studied by inelastic neutron scattering. *Z. Phys. B* **55**, 1–6 (1984).
23. F. Fillaux, B. Nicolaï, W. Paulus, Collective rotational tunneling of methyl groups and quantum solitons in 4-methylpyridine: Neutron scattering studies of single crystals. *Phys. Rev. B* **68**, 224301 (2003).
24. S. Khazaei, D. Sebastiani, Tunneling of coupled methyl quantum rotors in 4-methylpyridine: Single rotor potential versus coupling interaction. *J. Chem. Phys.* **147**, 194303 (2017).
25. L. Berliner, G. Hanson, Metals in biology: Applications of high-resolution EPR to metalloenzymes, in *Biological Magnetic Resonance* (Springer Science and Business Media, 2010), vol. 29, pp. 345-409.
26. Y. Xue, M. S. Pavlova, Y. E. Ryabov, B. Reif, N. R. Skrynnikov, Methyl rotation barriers in proteins from ^2H relaxation data. Implications for protein structure. *J. Am. Chem. Soc.* **129**, 6827–6838 (2007).
27. J. I. Martinez, P. J. Alonso, I. Garcia-Rubio, M. Medina, Methyl rotors in flavoproteins. *Phys. Chem. Chem. Phys.* **16**, 26203–26212 (2014).
28. S. Clough, J. R. Hill, M. Punkkinen, Slow methyl group tunneling rotation frequency measurements by electron nuclear double resonance. *J. Phys. C Solid State Phys.* **7**, 3779–3784 (1974).
29. T. D. Ladd, F. Jelezko, R. Laflamme, Y. Nakamura, C. Monroe, J. L. O'Brien, Quantum computers. *Nature* **464**, 45–53 (2010).
30. F. Bussières, N. Sangouard, M. Afzelius, H. de Riedmatten, C. Simon, W. Tittel, Prospective applications of optical quantum memories. *J. Mod. Optics* **60**, 1519–1537 (2013).
31. S. Van Doorslaer, G. A. Sierra, A. Schweiger, Dead time-dependent line distortions in absolute-value electron spin echo envelope modulation spectra. *J. Magn. Reson.* **136**, 152–158 (1999).
32. S. Stoll, A. Schweiger, EasySpin, a comprehensive software package for spectral simulation and analysis in EPR. *J. Magn. Reson.* **178**, 42–55 (2006).
33. M. J. Frisch, G. W. Trucks, H. B. Schlegel, G. E. Scuseria, M. A. Robb, J. R. Cheeseman, G. Scalmani, V. Barone, G. A. Petersson, H. Nakatsuji, X. Li, M. Caricato, A. Marenich, J. Bloino, B. G. Janesko, R. Gomperts, B. Mennucci, H. P. Hratchian, J. V. Ortiz, A. F. Izmaylov, J. L. Sonnenberg, D. Williams-Young, F. Ding, F. Lipparini, F. Egidi, J. Goings, B. Peng, A. Petrone, T. Henderson, D. Ranasinghe, V. G. Zakrzewski, J. Gao, N. Rega, G. Zheng, W. Liang, M. Hada, M. Ehara, K. Toyota, R. Fukuda, J. Hasegawa, M. Ishida, T. Nakajima, Y. Honda, O. Kitao, H. Nakai, T. Vreven, K. Throssell, J. A. Montgomery, Jr., J. E. Peralta, F. Ogliaro, M. Bearpark, J. J. Heyd, E. Brothers, K. N. Kudin, V. N. Staroverov, T. Keith, R. Kobayashi, J. Normand, K. Raghavachari, A. Rendell, J. C. Burant, S. S. Iyengar, J. Tomasi, M. Cossi, J. M. Millam, M. Klene, C. Adamo, R. Cammi, J. W. Ochterski, R. L. Martin, K. Morokuma, O. Farkas, J. B. Foresman, D. J. Fox Gaussian 09 Revision D.01, 2009 (Gaussian Inc., 2009).
34. F. Neese, Software update: The ORCA program system, version 4.0. *Wiley Inter. Rev. Comput. Mol. Sci.* **8**, e1327 (2018).

Acknowledgments: We thank High Performance Computing Center "HPC Sauletekis" of Vilnius University Faculty of Physics for the computational resources. **Funding:** G.J. acknowledges support by Swiss National Science Foundation grant 206021_157665.
Author contributions: Conceptualization: M.Š., D.K., J.B., A.P., and G.J. Data curation: M.Š. and D.K. Formal analysis: M.Š., D.K., and G.J. Funding acquisition: J.B. and G.J. Investigation: M.Š., D.K., K.A., and G.J. Methodology: M.Š., D.K., and G.J; Project administration: J.B., A.P., and G.J. Resources: M.P., M.M., and G.J. Software: D.K. and G.J. Supervision: J.B., A.P., and G.J. Validation: G.J. Visualization: D.K. and G.J. Writing—original draft: M.Š., D.K., and G.J. Writing—review and editing: all authors. **Competing interests:** The authors declare no competing interests. **Data and materials availability:** All data needed to evaluate the conclusions in the paper are present in the paper and/or the Supplementary Materials. Additional data related to this paper may be requested from the authors. The custom code that supports the findings of this study is available from the corresponding author upon request.

Submitted 8 November 2019
Accepted 4 February 2020
Published 1 May 2020
10.1126/sciadv.aba1517

Citation: M. Šimėnas, D. Klose, M. Ptak, K. Aidas, M. Mączka, J. Banys, A. Pöppl, G. Jeschke, Magnetic excitation and readout of methyl group tunnel coherence. *Sci. Adv.* **6**, eaba1517 (2020).

Science Advances

Magnetic excitation and readout of methyl group tunnel coherence

M. Simenas, D. Klose, M. Ptak, K. Aidas, M. Maczka, J. Banys, A. Pöppl and G. Jeschke

Sci Adv **6** (18), eaba1517.
DOI: 10.1126/sciadv.aba1517

Science Advances (ISSN 2375-2548) is published by the American Association for the Advancement of Science, 1200 New York Avenue NW, Washington, DC 20005. The title *Science Advances* is a registered trademark of AAAS.